Nucleon-nucleus scattering: a test of neutron matter

K. Amos

School of Physics, University of Melbourne, Victoria 3010, Australia

Abstract:- Using g-folding optical potentials, predictions of integral and angular observables from proton elastic scattering are used to assess model forms of neutron distributions in the target nuclei. ^{40,42,44,48}Ca and ^{208}Pb are used as examples.

I. INTRODUCTION

Usually nucleon-Nucleus (NA) elastic scattering data, total as well as angular dependent observables, have been analyzed using NA optical potentials; potentials most commonly taken to be local in form and often to have Woods-Saxon character. However, it has long been known that the optical potential must be nonlocal and markedly so, although it has been assumed also that the energy dependence of the customary (phenomenological) model accounts for that. Of more concern is that the phenomenological approach is not truly predictive. The parameter values chosen, while they may be set from a global survey of data analyses, are subject to uncertainties and ambiguities. While differential cross sections may be described by such local potentials, different parameter sets that are known to give similar results [1] may lead to different predictions for the total reaction cross section. There is no requirement that those diverse potentials be phase equivalent only that they lead to equivalent differential cross sections.

In contrast to analyses made using phenomenological local form interactions, I report on predictions found on using, complex, nonlocal, optical potentials formed in coordinate space. They are formed by folding realistic, effective, nucleon-nucleon (NN) interactions with density matrices (hereafter simply termed densities) of the nucleus; densities defined from credible nucleonic models of nuclear structure. All details of this approach have been given in a review [2]. Thus I give only those features relevant to the matters reported herein. For brevity, I identify hereafter the method used, and the optical potentials that result, by the term g-folding.

With this coordinate space approach, all analyses have been made using the program, DWBA98, of Jacques Raynal. That program allows the projectile-target nucleon (effective) interactions not only to be complex but also energy and density dependent; the latter being specific to the target in question. The properties of (nonlocal) optical potentials arise from mapping effective interactions to NN g matrices that are solutions of the Brueckner-Bethe-Goldstone (BBG) equations in nuclear matter, hence the origin of the term g-folding. The Bonn-B NN potentials have been used as input to solving those BBG equations. As the BBG equations allow for Pauli blocking and for a medium influence in the propagators, the ensuing effective NN interactions are nuclear density dependent. For each nucleus that effective interaction is selected according to the density the two nucleons experience on average for each pair of coordinates. Details again can be found in the review [2]. Such density dependence has been shown to be critical in making good predictions of angular and integral observables, including all spin observables, for intermediate energy nucleon scattering from all nuclei [2, 3]. As will be shown, the strong medium dependence varies with energy also with predictions of total reaction cross sections.

To define the nonlocal interaction for NA scattering in a full folding model, antisymmetry of the wave functions for the projectile and each and every bound nucleon wave function need be taken in the evaluation of multi–particle matrix elements of the (symbolic) form

$$U_{pA} = \left(\Psi\left(1 \ldots A\right) \left| \sum_{N=1}^{A} V_{N0} \right| \Psi\left(1 \ldots A\right) \right) \tag{1}$$

with $\langle \mathbf{R} | \ \Psi\left(1 \ldots A\right) \rangle$ being the many-body wave function for the ground state of the target and '0' denoting the projectile coordinates. As all nucleons in the target are equivalent, it is useful to choose a specific entry ("1") and write

$$U_{pA} = A \left(\Psi\left(1 \ldots A\right) \right| V_{10} \left| \Psi\left(1 \ldots A\right) \right) \ . \tag{2}$$

With the many-body state expanded in cofactors,

$$\left| \Psi\left(1 \ldots A\right) \right\rangle = \frac{1}{\sqrt{A}} \sum_{\alpha m} \left| \varphi_{\alpha m}(1) \right\rangle a_{\alpha m} \left| \Psi\left(1 \ldots A\right) \right\rangle \tag{3}$$

where α specifies the set of single particle (SP) quantum numbers $\{n, l, j, \zeta\}$ in which ζ is the isospin projection, the Eq. (2) becomes the functional

$$U_{pA}(0,1) = \sum_{\alpha m \alpha' m'} \left\langle \Psi \left| a^{\dagger}_{\alpha' m'} a_{\alpha m} \right| \Psi \right\rangle \left(\varphi_{\alpha' m'}(1) \right| V_{10} \left\{ \left| \varphi_{\alpha m}(1) \right\rangle - \left| \varphi_{\alpha m}(0) \right) \right\} \ , \tag{4}$$

when the antisymmetry between the projectile and struck nucleon is taken into account. The nuclear structure information required to evaluate the optical potentials are the many-body matrix elements of the particle-hole operators. They are defined by

$$\begin{aligned} \rho^{mm' M_i M_f}_{\alpha\alpha' J_i J_f} &= \left\langle \Psi \left| a^{\dagger}_{\alpha' m'} a_{\alpha m} \right| \Psi \right\rangle \\ &= \sum_{I,N} \frac{(-1)^{j-m}}{\sqrt{2J_f + 1}} \left\langle j\, m\, j' \ - m' \right| I \ - N \rangle \ \left\langle J_i\, M_i\, I\, N \right| J_f\, M_f \rangle \ S_{\alpha\alpha' I} \end{aligned} \tag{5}$$

where the $S_{\alpha\alpha' I}$ are one body density matrix elements (OBDME). With $\tilde{a}_{\alpha m} = (-1)^{j-m} a_{\alpha -m}$,

$$S_{\alpha\alpha' I} = \left\langle \Psi_{J_f} \left\| \left[a^{\dagger}_{\alpha'} \times \tilde{a}_{\alpha} \right]^I \right\| \Psi_{J_i} \right\rangle \rightarrow \left\langle \Psi_{J} \left\| \left[a^{\dagger}_{\alpha'} \times \tilde{a}_{\alpha} \right]^I \right\| \Psi_{J} \right\rangle \ . \tag{6}$$

In the elastic scattering case and from a target with zero spin, the OBDME reduce often to be the shell occupancies of the target. But if the ground state spin, J, is nonzero, scattering amplitudes with angular momentum transfer values from 0 to $I_{max}(= 2J)$ can contribute to elastic scattering. However, the contributions of the amplitudes with $I \neq 0$ are small and they can be treated well in a DWA by forming their scattering probabilities separately and adding the results incoherently to those derived from an optical potential specified by solely the OBDME with $I = 0$. As a result, one obtains a characteristic form for the optical potential

$$\begin{aligned} U(\mathbf{r_0}, \mathbf{r_1}; E) \ = \ \sum_{\alpha m \alpha' m'} (2j+1) S_{\alpha\alpha' 0} \Big[\delta(\mathbf{r_0} - \mathbf{r_1}) \int \varphi^*_{\alpha' m'}(\mathbf{s}) U^D(R_{0s}, E) \varphi_{\alpha m}(\mathbf{s}) \ d\mathbf{s} \\ + \varphi^*_{\alpha' m'}(\mathbf{r_1}) U^{Ex}(R_{01}, E) \varphi_{\alpha m}(\mathbf{r_0}) \Big] \ , \end{aligned} \tag{7}$$

where $R_{01} = |\mathbf{r_0} - \mathbf{r_1}|$, and U^D and U^{Ex} are appropriate combinations of the multipoles of the effective interaction for the direct and exchange contributions to the optical potential respectively [2].

The nuclear ground state densities are to be generated from nucleon-based models of structure. For example, for ^{12}C a complete $(0+2)\hbar\omega$ shell model [3] with the WBT interaction of Warburton and Brown [4] has been used. As another example, in some calculations with ^{208}Pb, Skyrme-Hartree-Fock wave functions [5] have been considered. But the key features of those structure models for use in forming g-folding optical potentials are the OBDME and the SP wave functions. They are also the primary features in defining the size of a nucleus, what 'skin thickness' there may be, and the variation of matter densities through the surface region. However, as the crucial roles of using large space (shell) model calculations of the spectra of nuclei and of the choice of SP wave functions has been highlighted in another presentation [6], I do not expand further herein.

I note in passing that inelastic scattering processes may be more influenced by the matter distributions through the nuclear surface of a target. To use inelastic scattering data to test such properties however one needs a predictive scattering theory. Presuming that is a DWA, then it is possible to specify a no parameter method of inelastic scattering data analysis by using the wave solutions of Schrödinger equations given by the g-folding optical potentials as the distorted wave functions, taking the same effective NN interaction potential as the inelastic transition operator, and nuclear structure input being again the bound state wave functions. The OBDME now are for the transition in question. With the light masses considered to date, large space no-core shell model calculations give transition OBDME that need little or no core polarization corrections. The propriety of this DWA is evident from numerous examples given in the review [2]. Both magnitudes and shapes of the data (differential cross sections and analyzing powers) are well reproduced. Coupled with elastic scattering analyses, using this prescribed method to analyze data from the inelastic scattering of ^{6}He ions from hydrogen is convincing evidence of a halo characteristic to the neutron density distribution in that ion [7].

II. ANGULAR DEPENDENT OBSERVABLES AND PREDICTIONS

Differential cross sections, and in some cases analyzing powers, from the scattering of nucleons from nuclei (and by inverse kinematics, of nuclei from hydrogen), reflect specific properties of the structure input to the analyses [2]. With elastic scattering it seems that data, typically taken at momentum transfers of 1 fm^{-1} and greater, with cross section values typically of the order of a mb/sr, are quite sensitive to the surface matter densities of the nucleus involved. Two studies are reported.

A. Probing the matter profiles of the Ca isotopes

I consider two model structures for the ground states of the isotopes ^{40,42,44,48}Ca herein. Other structures have been presented by Steven Karataglidis [6]. The first of the two I consider is a standard shell model, such as the oscillator (HO) model specified by Karataglidis and Chadwick [8]. With that scheme, ^{40}Ca is taken as a closed shell nucleus and ^{42,44,48}Ca have the extra 2, 4 and 8 neutrons respectively occupying the $0\hbar\omega$ space of f$_{7/2}$-f$_{5/2}$-p$_{3/2}$-p$_{1/2}$ orbits. The state occupancies were found using an oscillator length of 2.0 fm though a smaller value leads to a better proton scattering form factor in ^{40}Ca.

The second is the Skyrme-Hartree-Fock (SHF) model which has been used to give structure ground state wave functions for ^{40,44,48}Ca. The model densities used were those from

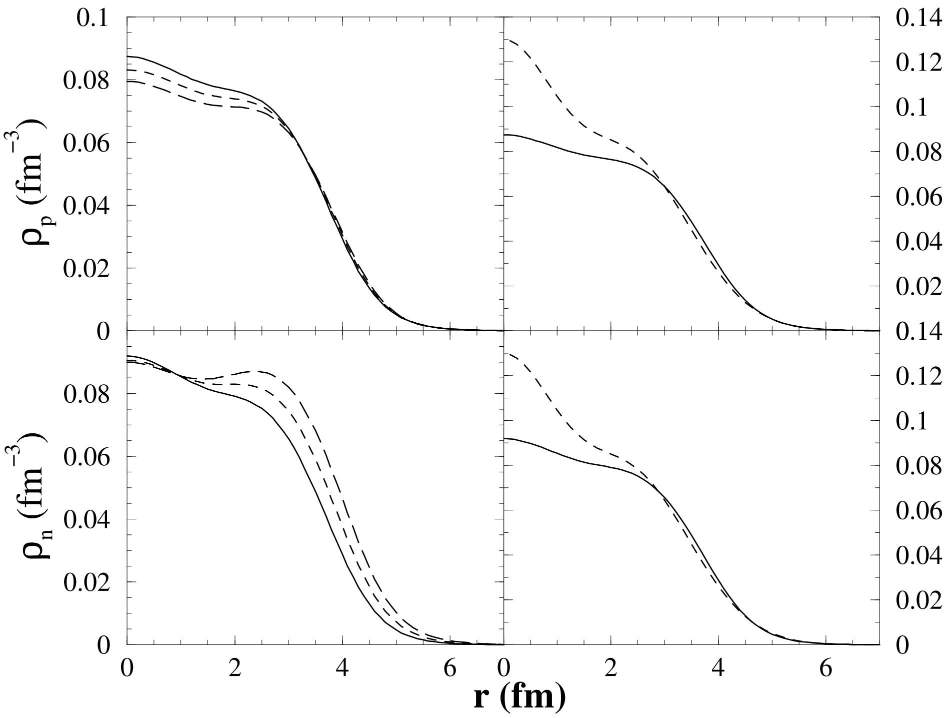

FIG. 1: The proton (top) and neutron (bottom) matter densities for isotopes of Ca. In the left side panels, the SHF/SKX model results for ^{40,44,48}Ca are shown by the solid, dashed and long dashed curves respectively. On the right the SHF/SKX and the HO results for ^{40}Ca are displayed by the solid and dashed curves respectively.

calculations made taking spherical closed-shell configurations [9]. Specifically I consider the results obtained by using the Skyrme interaction that has been denoted as SKX.

The separate proton and neutron densities from these model calculations are shown in the top and bottom segments of Fig. 1. In the left side panels, the SHF/SKX densities for the three isotopes are displayed. Clearly as neutrons are added the neutron matter density increases largely as result of more f-shell occupation. The proton density (for the fixed number of protons) is slightly extended as the mass increases, due to the nett attractive forces between those protons and the extra neutrons in ^{44,48}Ca. But that redistribution (of the protons) effects at most a 1% change to the proton root-mean-square (rms) radius. However, the additional neutrons largely are distributed at the surface to effect a neutron skin in both ^{44,48}Ca.

In the right side panels, the matter densities for ^{40}Ca given by the SHF/SKX model (solid curves) are compared with those given by the HO model (dashed lines). In the surface region, the two models predict essentially the same densities. As those densities differ markedly only well within the nuclear volume, one might expect to note influence on scattering results primarily at high momentum transfers and at energies for which absorption through the nucleus is not too large. Then differences should be evident in calculations of cross sections for scattering (from ^{40}Ca) at energies $\geq$ 200 MeV and at momentum transfer values ≥ 1 fm^{-1}.

The 65 and 200 MeV elastic scattering scattering cross sections for ^{40}Ca are displayed

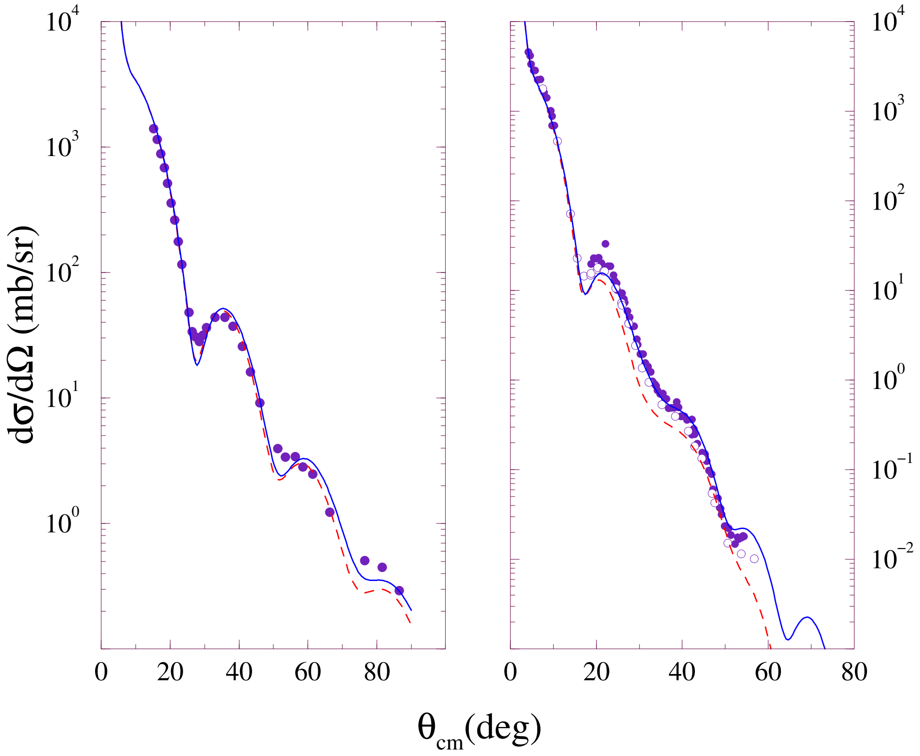

FIG. 2: Differential cross sections for the scattering of 65 MeV (left) and 200 MeV (right) protons from ^{40}Ca. Solid and dashed curves depict results found using the SHF/SKX and HO structures.

in Fig. 2. The agreement between the calculated results and the proton scattering data is very good. While at 65 MeV there is a slight preference for the SHF/SKX result at larger angles, it is with 200 MeV scattering that significant differences between the predictions of scattering made using the SHF/SKX and HO models are evident. Clearly the SHF/SKX model result agrees well with the data and is a significant improvement on the result found using the HO model.

The cross sections for 30.3 MeV proton elastic scattering from the three Ca isotopes are presented in Fig. 3. Therein the results given in top, middle and bottom segments are the cross sections from ^{40}Ca, ^{44}Ca, and ^{48}Ca respectively. The data are compared with the predictions found with the HO model of structure (dot-dashed curves) and with the SHF model structure (solid curves) for ^{40,44,48}Ca. Clearly the general trends in magnitudes and peak heights and positions are given by the calculated results but details are not matched as well as they have been at higher energies for ^{40}Ca, using the same scattering theory. Nor are they as good as predictions at this energy for scattering from other nuclei. Such may well be evidence of the character of the targets, and their excitation spectra specifically in the vicinity of 30 MeV, playing a role more complex than has been assumed in specifying the effective NN interaction.

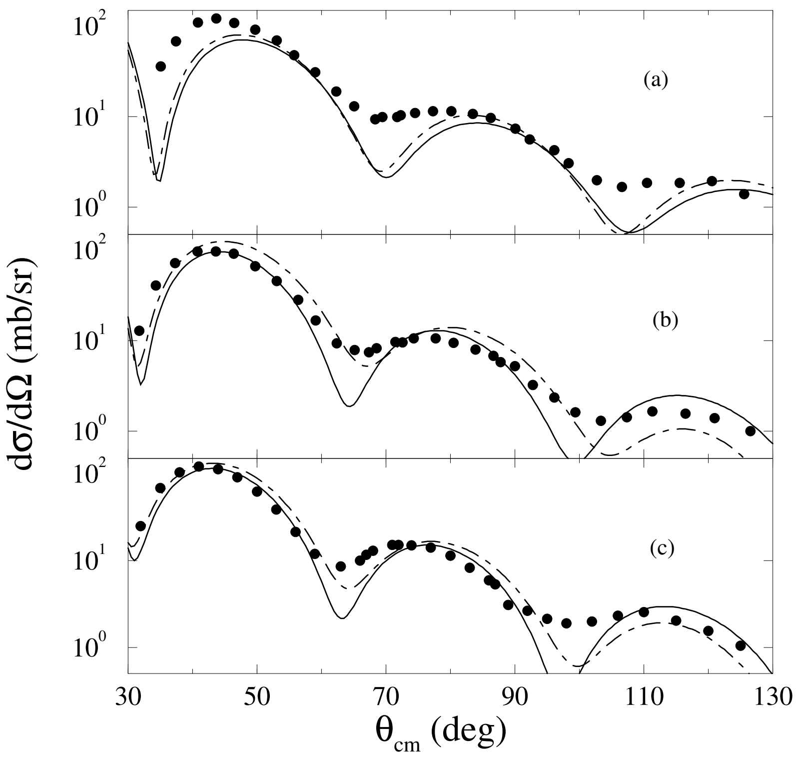

FIG. 3: Differential cross sections for the scattering of 30.3 MeV protons from ^{40,44,48}Ca. Solid and dot-dashed curves depict results found using the SHF/SKX and HO structures.

B. Probing the matter profiles of ^{208}Pb

Studies of the matter distributions of ^{208}Pb, and of its neutron density profile particularly, are quite topical. Indeed to specify its neutron rms radius is the aim of a parity violation electron scattering experiment. In contrast to proton rms radii that are known to within an accuracy of ~ 0.02 fm, neutron rms radii at best are known to an accuracy of ~ 0.2 fm. Lately, however, the neutron rms radius in ^{208}Pb was assessed in terms of modern SHF models of structure [5]. With the Friedman-Pandharipande neutron equation of state as constraint, the neutron rms radius in ^{208}Pb is expected to be 0.16 ± 0.02 fm larger than the proton value. Previous estimates of this neutron skin, $S = \sqrt{\langle r_n^2 \rangle} - \sqrt{\langle r_p^2 \rangle}$, ranged from 0.1 fm to 0.3 fm; the lower values favored in general by SHF models while relativistic mean field models predict values closer to 0.3 fm. Knowledge of the ^{208}Pb skin thickness then will be an important condition upon such models. Recently [10], proton scattering was studied seeking to select between a commonly used prescription for ^{208}Pb, i.e. of a packed shell nucleus with oscillator functions, the HO model, and more detailed SHF prescriptions [5]. The oscillator energy $\hbar\omega$ for the neutron states was 7.2 MeV so that both this HO model and a SHF model (built upon the SKX force) had the same nucleon rms radii (5.45 fm for protons and 5.61 fm for neutrons). Of course there are differing SHF results according to the base interaction used. The SHF result (SHF/SKM*) was found using an older force that gave a skin thickness of 0.17 fm.

The density profiles are more distinct. As reported [10], while all SHF results are similar

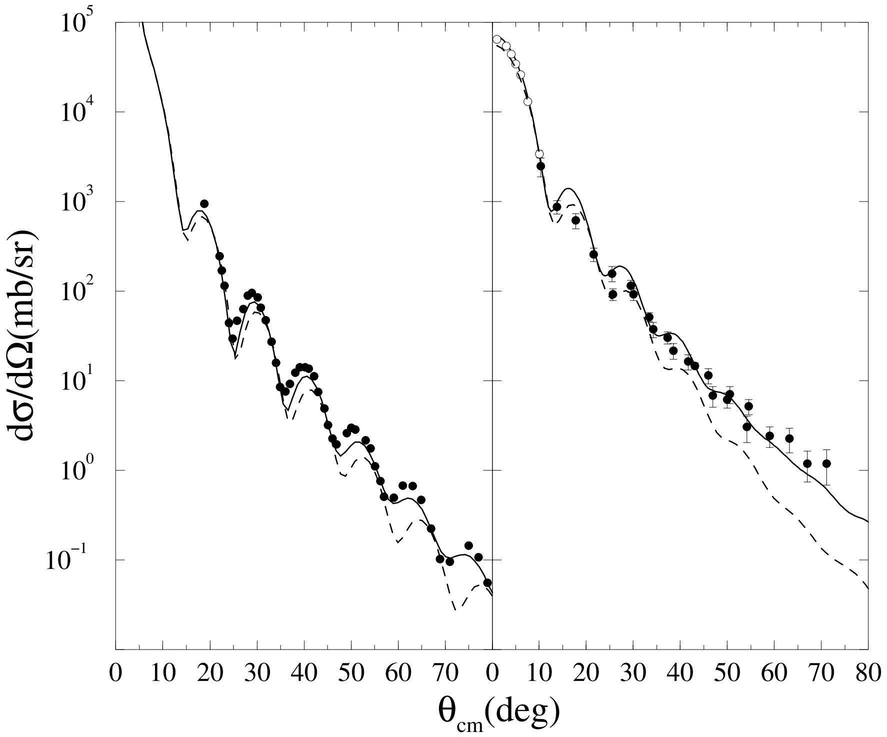

FIG. 4: Differential cross sections from 100.4 MeV protons (left) and 96 MeV neutrons (right) scattering from ^{208}Pb. Curves are identified in the text.

in form, the differences between the HO and any SHF results are most pronounced; and that is despite the rms radii being very similar. Details of the proton mass variation is most readily reflected by use of these structures to predict longitudinal form factors from electron scattering. Those form factors were presented previously [10] and clearly the HO result was quite different to any of the SHF model results. The HO model form factor also was a poor match to the data. Not so all of the SHF results at least to 1.5 fm^{-1}. However, of the three, the SHF/SKM* model gave the best match to data to 3.0 fm^{-1} and the differences between these SHF results in the range 1.5 to 3.0 fm^{-1} momentum transfer was quite evident. Differences also are evident in calculated proton elastic scattering cross sections when these structure models are used in forming g-folding optical potentials.

In Fig. 4, g-folding model predictions are compared with data from the scattering of 100.4 MeV protons (left) and of 96 MeV neutrons (right). The two predictions shown for each case, were found using the HO (dashed curve) and SHF/SKM* (solid curve) structure model information. Clearly only on using the SHF model structure is the data replicated, and that is so for both data sets. Since the isoscalar force, and in the $^3S_1$ channel particularly, is the strongest component in the effective interaction [2], the scattering of neutrons (protons) is most influenced by the proton (neutron) matter of the target nuclei. Consequently proton scattering can be sufficiently sensitive to the neutron matter distribution for cross sections to indicate which of the SHF models is the more reasonable. That can be seen from the results shown in Fig. 5. Therein predictions made using the HO (short dashed), the SHF/SKX (long dashed), and SHF/SKM* (solid) with measured data from 200 MeV proton elastic scattering from ^{208}Pb. Clearly the results differ, the SHF ones notably in the momentum transfer range 1.5 to 3 fm^{-1}, with the data revealing that the SHF/SKM* prescription is preferred. Indeed these analyses suggest that the skin thickness in ^{208}Pb should be slightly smaller.

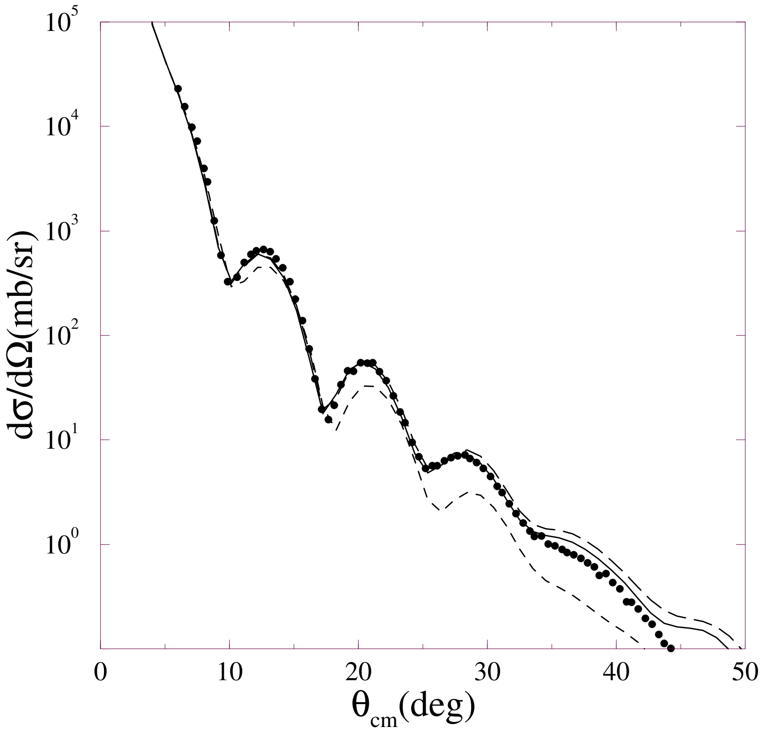

FIG. 5: Differential cross sections for 200 MeV protons on ^{208}Pb. Curves are identified in the text.

III. TOTAL CROSS SECTIONS

With $E \propto k^2$, the total reaction cross sections are defined by

$$\sigma_R(E) = \frac{\pi}{k^2} \sum_{l=0}^{\infty} \left\{ (l+1) \left[1 - \left(\eta_l^+ \right)^2 \right] + l \left[1 - \left(\eta_l^- \right)^2 \right] \right\} , \tag{8}$$

where $\eta_l^\pm$ are the moduli of S matrices that are determined from solutions of the radial Schödinger equations with the specified optical potentials. They are

$$\eta_l^\pm \equiv \eta_l^\pm(k) = \left| S_l^\pm(k) \right| = e^{-2\Im\left[\delta_l^\pm(k)\right]} , \tag{9}$$

where $\delta_l^\pm(k)$ are the scattering phase shifts and $\Im$ denotes the imaginary part. Using the sets of phase shifts determined from calculations with the g-folding optical potentials, proton reaction cross sections at many energies and for many targets have been analyzed successfully [3] Values for scattering of protons from the Ca isotopes have been measured and are compared with the results from g-folding calculations in the left panel of Fig. 6. Results from scattering of neutrons from diverse nuclei are shown in the right panel. So far only HO model studies of this data have been completed. The proton total reaction cross sections from the Ca isotopes are compared with predictions made using the HO model (with oscillator length

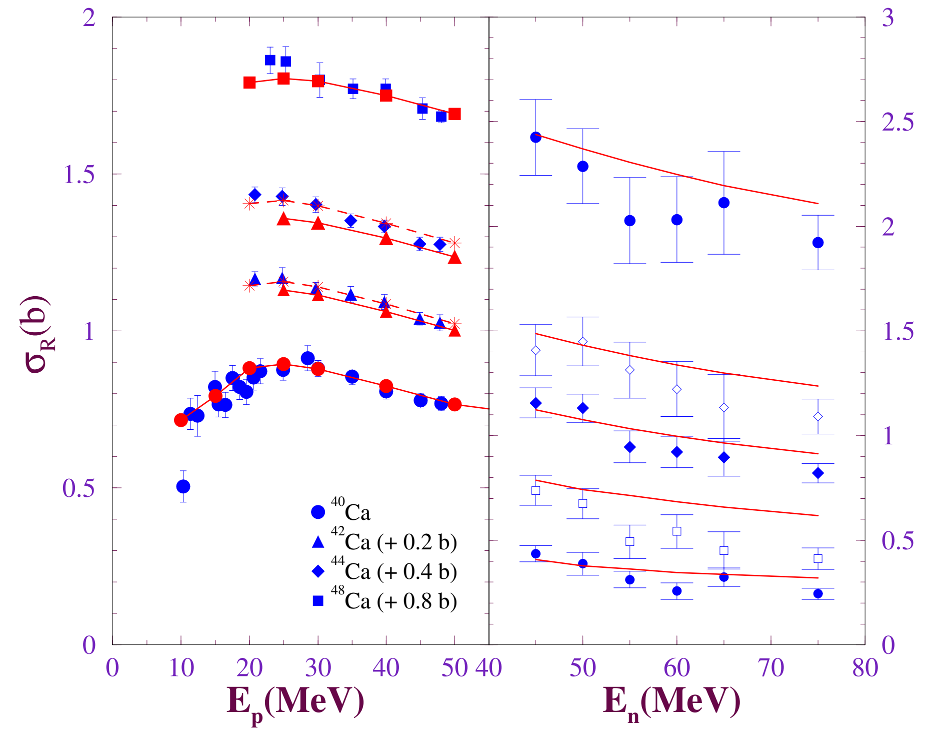

FIG. 6: Experimental values of σ_R (i) in the left panel for proton scattering from the Ca isotopes scaled as indicated and (ii) in the right side for neutron scattering from ^{12}C, ^{28}Si, ^{56}Fe, ^{90}Zr, and ^{208}Pb (in ascending sequence) compared with g-folding optical potential predictions.

, $b = 1.85$ fm) and displayed by the solid curves connecting the energy values at which actual numbers were obtained. The dashed curves (for ^{42,44}Ca) connect predictions made at the selected energies allowing the oscillator length to be 1.88 and 1.92 fm. respectively. Of note is that the trends of the data with mass and energy are well reproduced, even the low energy data (for ^{40}Ca). That is also the case with the neutron data from different nuclei spanning the mass table, as shown in the right panel of Fig. 6. Of course, the neutron data have sizable statistical error bars but nonetheless the energy and mass trends are well reproduced by the g-folding model predictions. But note that there appears to be a discrepancy in the case of ^{28}Si, where results tend to over-predict the data.

Finally, in Fig. 7, proton reaction cross sections to 200 MeV from ^{40}Ca (left panel) and from ^{208}Pb are shown. With ^{40}Ca, two calculated results are displayed. Both were made using the HO model structure (with $b = 1.85$ fm). The solid curve is the result found using the defined g-folding potential it reproduces the data very well, even giving the energy variation down to quite low energies. The dashed curve, on the other hand, is the result obtained when the medium dependences of the effective interaction were switched off, i.e. a t-folding potential was used. Clearly the medium modifications brought about by the Pauli blocking and an average mean field defining the propagators in the g matrix generation are crucial. The two results in the right hand panel were obtained using proper g-folding potentials for ^{208}Pb but the foldings were made with the HO model structure (dot-dashed curve) and with the SHF/SKM* model structure (solid curve). Clearly the results for the

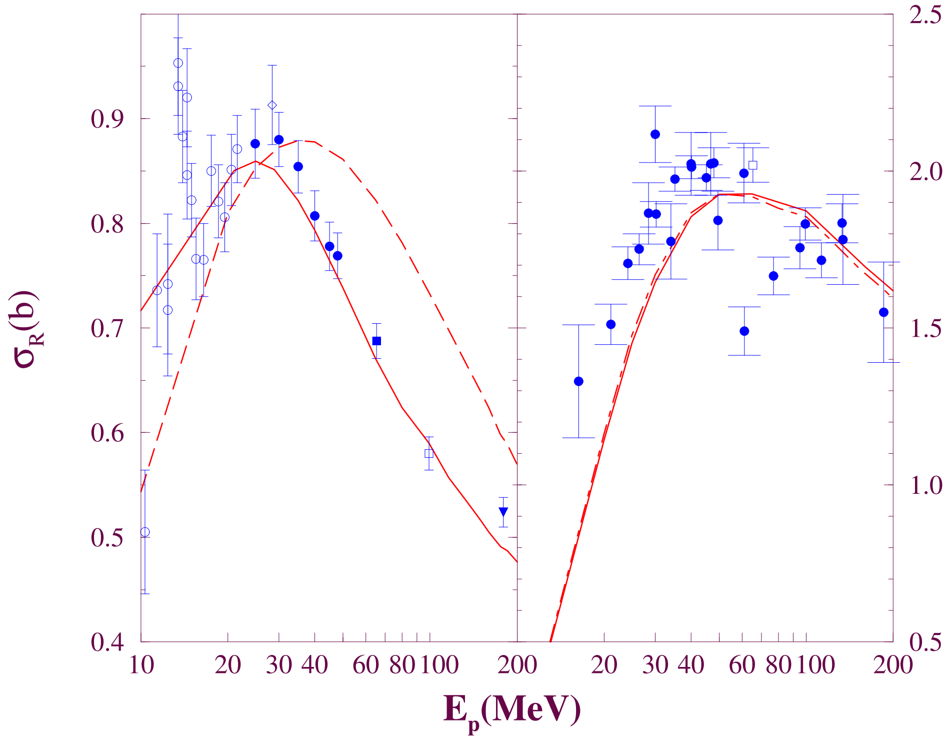

FIG. 7: Proton total reaction cross section data compared with g-folding optical potential results for ^{40}Ca (left) and ^{208}Pb (right).

reaction cross sections with both models (which have essentially the same proton and neutron rms radii) are nearly identical. They reflect the data above 60 MeV quite well but both fall below the data at lower energies in this case. The low value data points (60-70 MeV) are not thought to be valid.

Acknowledgments:–

This work was supported by a grant from the Australian Research Council.

[1] P. E. Hodgson, *The Nucleon Optical Potential* (World Scientific, Singapore, 1994).

[2] K. Amos, P. J. Dortmans, H. V. von Geramb, S. Karataglidis, and J. Raynal, Adv. in Nucl. Phys. **25**, 275 (2000), (and references cited therein).

[3] P. K. Deb, K. Amos, S. Karataglidis, M. B. Chadwick, and D. G. Madland, Phys. Rev. Lett. **86**, 3248 (2001).

[4] E. K. Warburton and B. A. Brown, Phys. Rev. C **46**, 923 (1992).

[5] B. A. Brown, Phys. Rev. Lett. **85**, 5296 (2000).

[6] S. Karataglidis (2003), contribution to this conference.

[7] S. V. Stepantsov et al., Phys. Letts. **542**, 35 (2002).

[8] S. Karataglidis and M. B. Chadwick, Phys. Rev. C **64**, 064601 (2001).

[9] B. A. Brown, Phys. Rev. C **58**, 220 (1998).

[10] S. Karataglidis, K. Amos, B. A. Brown, and P. K. Deb, Phys. Rev. C **65**, 044306 (2002).